



HAL
open science

Proof of Principle: Immobilisation of Robust Cu II 3 Tb III -Macrocycles on Small, Suitably Pre-functionalised Gold Nanoparticles

Humphrey L C Feltham, Christophe Dumas, Matteo Mannini, Edwige Otero, Philippe Saintavit, Roberta Sessoli, Carla J Meledandri, Sally Brooker

► **To cite this version:**

Humphrey L C Feltham, Christophe Dumas, Matteo Mannini, Edwige Otero, Philippe Saintavit, et al.. Proof of Principle: Immobilisation of Robust Cu II 3 Tb III -Macrocycles on Small, Suitably Pre-functionalised Gold Nanoparticles. *Chemistry - A European Journal*, 2017, 23 (11), pp.2517-2521. 10.1002/chem.201604821 . hal-03989107

HAL Id: hal-03989107

<https://cnrs.hal.science/hal-03989107>

Submitted on 14 Feb 2023

HAL is a multi-disciplinary open access archive for the deposit and dissemination of scientific research documents, whether they are published or not. The documents may come from teaching and research institutions in France or abroad, or from public or private research centers.

L'archive ouverte pluridisciplinaire **HAL**, est destinée au dépôt et à la diffusion de documents scientifiques de niveau recherche, publiés ou non, émanant des établissements d'enseignement et de recherche français ou étrangers, des laboratoires publics ou privés.

Single-Molecule Magnet behavior of a $\text{Cu}^{\text{II}}_3\text{Tb}^{\text{III}}$ macrocyclic complex immobilized on gold nanoparticles

Humphrey L. C. Feltham,[†] Christophe Dumas,[†] Matteo Mannini,[‡] Edwige Otero,[£] Philippe Sainctavit,^{£,¥} Roberta Sessoli,^{‡,*} Carla J. Meledandri^{†,*} and Sally Brooker^{†,*}

[†]Department of Chemistry and the MacDiarmid Institute for Advanced Materials and Nanotechnology, University of Otago, B.O. Box 56, Dunedin 9054, New Zealand

[‡]Dipartimento di Chimica “Ugo Schiff” and UDR INSTM, Università degli Studi di Firenze, Via della Lastruccia 3–13, 50019 Sesto Fiorentino, Italy.

[£] *Synchrotron SOLEIL, L’Orme des Merisiers, Saint-Aubin—BP 48, 91192 Gif-sur-Yvette, France*

[¥] *Institut de Mineralogie, de Physique des Matériaux et de Cosmochimie, UMR 7590, CNRS, UPMC, IRD, MNHN 75005 Paris, France*

KEYWORDS. *Single Molecule Magnet, gold, nanoparticle, surface, magnetism*

Supporting Information Placeholder

ABSTRACT: A highly stable and processable macrocyclic Single-Molecule Magnet (SMM) containing one Tb^{III} and three Cu^{II} ions in the core structure was covalently grafted onto gold nanoparticles pre-functionalised with carboxylate terminated tethers. The modified microemulsion method allowed production of small and monodisperse nanoparticles (about 3.5 nm in diameter) for the chemisorption of a huge amount of molecules, with retention of the SMM behavior in the final hybrid system.

Single-Molecule Magnets (SMMs) exhibit slow relaxation of magnetism that is of purely molecular origin.¹ In contrast to traditional bulk magnets, the observation of memory effects in SMMs is the result of anisotropy of the magnetization of “giant” spin based well isolated molecular systems rather than the energy cost associated with the reorganization of domain walls. Even though the temperatures below which SMMs² display the characteristic blocking of magnetization remain very low, SMMs still represent an ideal field to develop new tools to control the magnetization at the nanoscale.

Research aimed at immobilization of SMMs on solid supports is of key importance as in principle this would allow individual molecules to be addressed.³ To date, the two main compounds used for such experiments, with retention of SMM behavior in the resulting hybrid material, are bis(phthalocyanine)lanthanide(III) complexes (TbPc_2)⁴ and tetranuclear iron(III) complexes (Fe_4),^{5,6,7} that have been assembled in different nano-architectures. There are two main types of deposition of SMM⁸ (a) non-specific (simple/direct deposition eg. by sublimation or evaporation of a solution) and (b) covalent attachment, with the latter approach expected to give greater control of the molecule-substrate interaction as well as greater versatility. In the case of the Fe_4 complexes covalently attached to gold, the orientation/position of the complex relative to the surface, and hence the length of the tether separating the magnetic core and the substrate, was found to be important.⁶ This illustrates one of the key challenges in such studies: that the magnetic blocking is frequently lost when the SMM is immobilized on a surface,⁹ either due to the complex lacking sta-

bility (metal redox or ligand dissociation) or to the change in chemical environment experienced by the complex (pure crystalline solid vs interacting with a surface⁶). Moreover, characterizing the magnetic properties of an SMM on a surface usually requires highly-sensitive synchrotron-based techniques because of (a) the tiny quantities of sample present in a mono- or even multi-layer, and (b) immobilizing the complex on a ‘flat’ surface produces a sample that is not conducive to the sample holders of most standard in-house characterization methods. However, some of us reported that appropriately functionalized Fe_4 SMMs can be immobilized on monodisperse Au NPs, and that the resulting hybrid material can be characterized by standard SQUID methods.⁷ Muragesu and co-workers instead attached Dy_2 SMMs to “naked” gold nanoparticles (NPs) of a wide range of sizes (generated by laser ablation), then studied by standard methods, revealing a more pronounced change in the magnetization dynamics.¹⁰

As noted above, processable SMMs suitable for surface attachment are in limited supply. Hence we have used our expertise in macrocyclic chemistry to develop a large series of robust soluble tetranuclear 3d-4f macrocyclic complexes, $\text{M}^{\text{II}}_3\text{Ln}^{\text{III}}(\text{L}^{\text{R}})(\text{NO}_3)_3$, with SMM properties tuned by choice of the 3d and 4f ions and aliphatic linkers L^{R} .^{11,12} Of them, to date, $[\text{Cu}^{\text{II}}_3\text{Tb}^{\text{III}}(\text{L}^{\text{Bu}})(\text{NO}_3)_2(\text{MeOH})(\text{H}_2\text{O})](\text{NO}_3) \cdot 3\text{H}_2\text{O}$, referred to from here-on as $[\text{Cu}_3\text{Tb}(\text{L}^{\text{Bu}})]$ (see Figure 1), has shown the best SMM properties.¹² It features a relatively flat macrocycle which encircles the four metal ions, leading to a ‘plate-like’ cationic structure (Figure 1), with axial $\text{Tb}(\text{III})$ -nitrate and $\text{Cu}(\text{II})$ -solvent bonds completing the coordination and providing charge balance. The macrocyclic effect endows $[\text{Cu}_3\text{Tb}(\text{L}^{\text{Bu}})]$ with enhanced stability in solution, making it a good candidate for covalent tethering to surfaces, as it should retain its structure during this process.

The well-known dodecamanganese (III,IV), Mn_{12} SMM has previously been immobilized on silicon¹³ and gold¹⁴ surfaces pre-functionalized with anionic carboxylate tethers, albeit without confirmation of retention of SMM behavior. Similarly, we use an anionic carboxylate tether, α -lipoic acid (ALA), to facilitate binding to our cationic SMM, preferentially via central *hard* $\text{Tb}(\text{III})$ (Figure 1). In addition, the coordination of this tether helps to prevent unfavorable interactions between the SMM and the surface.

Importantly, the present study also demonstrates that the microemulsion method¹⁵ can be extended well beyond coating NPs with the long, aliphatic, non-polar molecules usually employed.¹⁶ Here tethers containing interesting functional groups, carboxylates, are attached to the surface, whilst retaining the key advantage of the microemulsion method: controlled formation of small monodisperse NPs. Previously one had (a) either NPs with interesting coatings *or* (b) controlled formation of small monodisperse NPs. Showing that we can have both opens up a plethora of new possibilities.

Herein we develop access to, and then employ, monodisperse gold NPs *pre-functionalized with anionic tethers* suitable for coordination to the *cationic robust SMM* $[\text{Cu}_3\text{Tb}(\text{L}^{\text{Bu}})]$, forming a new hybrid, $[\text{Cu}_3\text{Tb}(\text{L}^{\text{Bu}})]@Au$ (Figure 1), that *retains SMM behavior*.

Elaboration of the microemulsion method has provided access to the desired small ALA-coated gold nanoparticles, ALA@Au (Figure 1). Two heptane emulsions, comprising $\text{AuCl}_3(\text{aq})$ and $\text{NaBH}_4(\text{aq})$ reversible micelles (dioctyl sulfosuccinate surfactant), are mixed. The Au NPs grow inside the micelles, with their size controlled by the size of the micelles. To the resulting dispersion of surfactant-stabilized NPs is added ALA in ethanol. Acetone:methanol is then added to disrupt the micelles, so the ALA coated NPs, ALA@Au, precipitate and can be isolated. After washing several times with ethanol (to remove unreacted ALA), they are taken up in water (pH = 9) and centrifuged to remove aggregates. At pH 9, the ALA is in the anionic carboxylate form which facilitates the dispersion of ALA@Au in water (Dynamic Light Scattering gave a zeta potential of -50 mV). Transmission Electron Microscopy showed that monodisperse 3.6 ± 0.7 nm diameter NPs had been obtained (Figure S1), and UV-Vis spectroscopy showed a single surface plasmon absorption band at 526 nm, consistent with the presence of non-aggregated spherical gold nanoparticles of diameter less than 5 nm.¹⁷

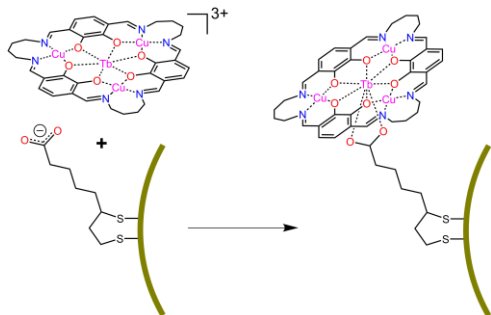


Figure 1. Reaction of the anionic ALA@Au NPs with a the cationic $[\text{Cu}_3\text{Tb}(\text{L}^{\text{Bu}})]$ SMM forming $[\text{Cu}_3\text{Tb}(\text{L}^{\text{Bu}})]@Au$ (showing a possible binding mode). For clarity, counter anions and the remaining ‘axial’ ligands in the coordination spheres of the metal ions are not shown.

The aqueous dispersion of ALA@Au is added dropwise to a DMF solution of $[\text{Cu}_3\text{Tb}(\text{L}^{\text{Bu}})]$ ¹² (Figure 1; both reagents are highly soluble in the reaction solvent mixture, and in DMF). A black precipitate forms over the next few days, which is isolated by centrifugation and washed with DMF, then methanol, before air drying. The resulting hybrid material, $[\text{Cu}_3\text{Tb}(\text{L}^{\text{Bu}})]@Au$, cannot be re-dispersed in common organic solvents, or water, even with sonication, which suggests aggregation of the nanoparticles by cross-linking. This insolubility precludes any solution-phase characterization.

A range of solid-state surface techniques have been used to confirm the integrity of the $[\text{Cu}_3\text{Tb}(\text{L}^{\text{Bu}})]$ immobilized on the surface of the Au NPs. X-ray Photoelectron Spectroscopy (XPS) per-

formed on pristine $[\text{Cu}_3\text{Tb}(\text{L}^{\text{Bu}})]$ (Figure S2) and $[\text{Cu}_3\text{Tb}(\text{L}^{\text{Bu}})]@Au$ (Figure 2 and S3) confirmed that both the ALA functionalization of AuNPs and the reaction described in Figure 1 have been successfully achieved. First of all the position in energy of the $S2p$ main peak (See Figure S2 in SI), found in both the ALA@Au and $[\text{Cu}_3\text{Tb}(\text{L}^{\text{Bu}})]@Au$ samples below 162 eV indicates the formation of Au-S covalent bonds. The decrease in intensity of the $S2p$ peak with respect to the Au4f signal could be justified by the presence of the SMM molecules that cover them in $[\text{Cu}_3\text{Tb}(\text{L}^{\text{Bu}})]@Au$ (see Table S1 in SI). Even more interesting are the results obtained by the investigation of the Tb3d and Cu2p regions that evidenced nearly identical absorptions corresponding to the Cu^{II} and Tb^{III} ions. Although the main Cu2p and Tb3d peaks are partially obscured by the Auger peaks of C and O, a semi-quantitative analysis was performed by the evaluation of the intensity of $\text{Cu}2p_{3/2}$ and $\text{Tb}3d_{3/2}$ peaks. In both $[\text{Cu}_3\text{Tb}(\text{L}^{\text{Bu}})]$ and $[\text{Cu}_3\text{Tb}(\text{L}^{\text{Bu}})]@Au$, the analysis yielded a 3:1 ratio of $\text{Cu}^{\text{II}}:\text{Tb}^{\text{III}}$, as expected for the intact tetranuclear $\text{Cu}^{\text{II}}_3\text{Tb}^{\text{III}}$ motif (see table S1 in the SI).

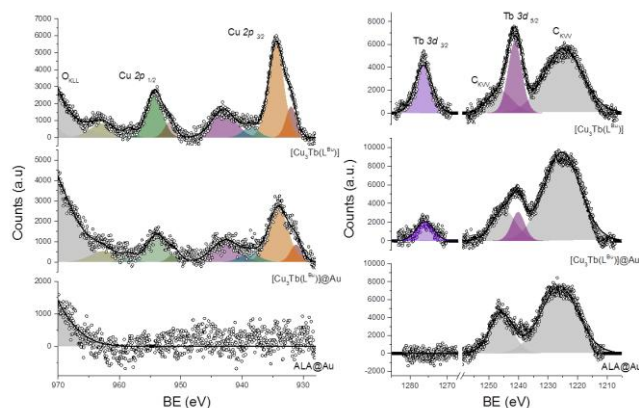


Figure 2. High resolution XPS spectra of the $\text{Cu}2p$ (left) and $\text{Tb}3d$ (right) region in $[\text{Cu}_3\text{Tb}(\text{L}^{\text{Bu}})]$ bulk sample, $[\text{Cu}_3\text{Tb}(\text{L}^{\text{Bu}})]@Au$, ALA@Au. A linear baseline has been subtracted to compare the spectra. The reported components have been used to fit the data and to extract the semi-quantitative information reported in Table S1.

Next, the magnetic properties of $[\text{Cu}_3\text{Tb}(\text{L}^{\text{Bu}})]@Au$ were probed by standard SQUID magnetometry. First, the proportion of $[\text{Cu}_3\text{Tb}(\text{L}^{\text{Bu}})]$ in $[\text{Cu}_3\text{Tb}(\text{L}^{\text{Bu}})]@Au$ was determined, by consideration of the susceptibility data above 50 K (above the energy of the exchange interactions), to be 36-39% (for details see Section 4, SI). This is in reasonable agreement with the ballpark percentage predicted by theoretical surface coverage calculations (28%, for details see Section 5, SI). With the percentage of $[\text{Cu}^{\text{II}}_3\text{Tb}^{\text{III}}(\text{L}^{\text{Bu}})]$ in $[\text{Cu}^{\text{II}}_3\text{Tb}^{\text{III}}(\text{L}^{\text{Bu}})]@Au$ in hand, the gram susceptibility data (Figure S7) can be re-scaled to allow for 37% SMM content. This facilitates comparison with the pure SMM and reveals similar behavior (Figure 3).¹²

From 50-280 K the precise shape of the curve for $[\text{Cu}_3\text{Tb}(\text{L}^{\text{Bu}})]@Au$ (Figure 3) depends on how the contribution of the ALA@Au (Figure S8) is corrected for (Section 4 of the Supporting Information). In Figure 3 we report uncorrected data (green squares) and those when $63\% \times \chi_g$ of ALA@Au data are subtracted from the χ_g data for $[\text{Cu}_3\text{Tb}(\text{L}^{\text{Bu}})]@Au$ (blue triangles). Though differences are observed at high temperature between the two sets the low temperature data superimpose, so the key features in that region remain clear. Specifically, below about 40 K there is a clear increase in $\chi_g T$, consistent with ferromagnetic in-

interactions between the $\text{Tb}^{\text{III}}\text{-Cu}^{\text{II}}$ and $\text{Cu}^{\text{II}}\text{-Cu}^{\text{II}}$ centers. The $\chi_g T$ product ultimately reaches a maximum at 4 K, the same temperature as in the free $[\text{Cu}_3\text{Tb}(\text{L}^{\text{Bu}})]$, before decreasing again to 1.8 K, in agreement with the presence of a highly anisotropic Tb^{III} ion. The increase is not as pronounced as that observed for the free SMM, but this subtle change is likely a consequence of binding of this SMM to the NP. The presence of anisotropic Tb^{III} is confirmed by the field dependence of magnetization of $[\text{Cu}_3\text{Tb}(\text{L}^{\text{Bu}})]@Au$, which shows non-saturation even at 1.8 K and 70 kOe (Figure S9).

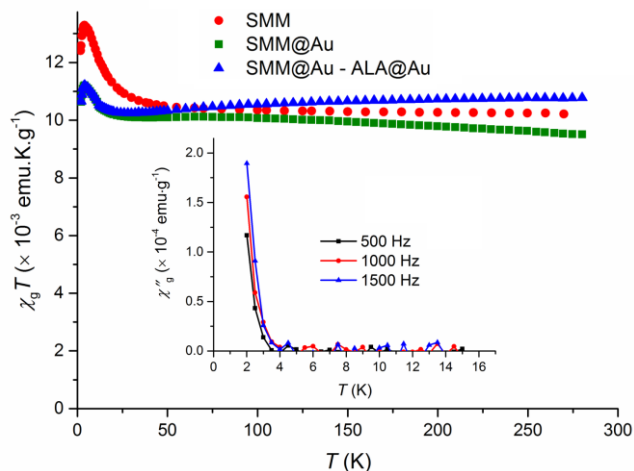


Figure 3. Temperature dependence of the $\chi_g T$ product in a 1000 Oe dc field for: $[\text{Cu}_3\text{Tb}(\text{L}^{\text{Bu}})]$ in red circles, and $[\text{Cu}_3\text{Tb}(\text{L}^{\text{Bu}})]@Au$ shown in two ways: green squares (data simply re-scaled by the estimated percentage, 37%, of $[\text{Cu}_3\text{Tb}(\text{L}^{\text{Bu}})]$ in $[\text{Cu}_3\text{Tb}(\text{L}^{\text{Bu}})]@Au$) and blue triangles (data corrected for the 63% contribution of ALA@Au). See Supporting Information for details and expansion of low temperature region. Inset: Temperature dependence of the out-of-phase component of ac susceptibility of $[\text{Cu}_3\text{Tb}(\text{L}^{\text{Bu}})]@Au$ at 1.8 K, alternating at the frequencies indicated. The solid lines are simply a guide for the eye.

To verify that the low temperature upturn in the χT is a fingerprint of intact SMMs functionalizing the Au NP, X-ray Absorption Spectroscopy (XAS) and X-ray Magnetic Circular Dichroism (XMCD) studies were performed on $[\text{Cu}_3\text{Tb}(\text{L}^{\text{Bu}})]@Au$ at 2 K (Figure 4a,b) at the $L_{2,3}$ edges of Cu and the $M_{4,5}$ edges for Tb. Spectral features remained identical to that of the pristine SMM (Figure S5). Sum rules approach (see Supporting Information for details) confirm that the orbital μ_L and spin μ_S magnetic moments of Cu^{II} and Tb^{III} ions are almost unaltered with respect to the bulk and the resulting magnetic moments are in line with bulk SQUID measurements (see Table S2). Noticeable is the attenuation of the resulting total magnetic moment of Tb confirming the previous ab initio analysis [Feltham Inorg chem 2012]. XMCD element selectivity has been also used to measure magnetization curve of the Cu(II) ions by monitoring the dependence of the dichroism at the Cu edge as a function of the magnetic field. This does not follow the expected Brillouin curve for uncoupled Cu(II) ions. In addition, it is practically superimposable with that recorded at Tb edges and with the SQUID magnetic data for $[\text{Cu}_3\text{Tb}(\text{L}^{\text{Bu}})]$. This observation confirms ferromagnetic $\text{Cu}^{\text{II}}\text{-Tb}^{\text{III}}$ coupling typical of intact tetranuclear units.¹²

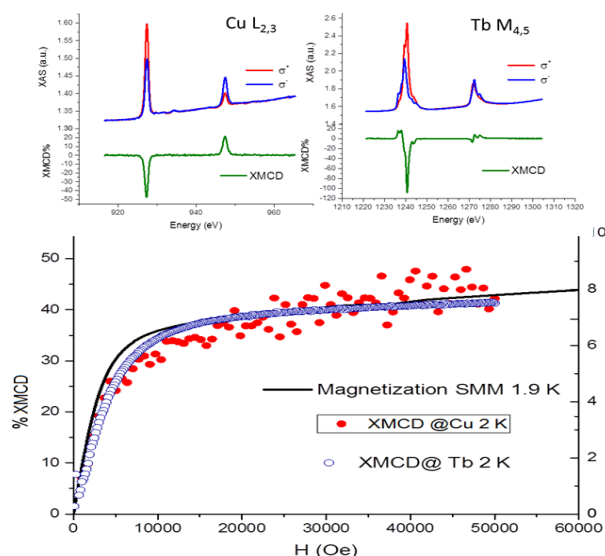


Figure 4. a,b) Tb and Cu XAS and XMCD data for the $[\text{Cu}_3\text{Tb}(\text{L}^{\text{Bu}})]@Au$ hybrid. c) Comparison of the XMCD data at 2 K (red circles = Cu edge, hollow circles = Tb edge) for $[\text{Cu}_3\text{Tb}(\text{L}^{\text{Bu}})]@Au$ NP and SQUID data for pure $[\text{Cu}_3\text{Tb}(\text{L}^{\text{Bu}})]$ at 1.9 K (black line).

Finally, the ac magnetic properties of the new hybrid, $[\text{Cu}_3\text{Tb}(\text{L}^{\text{Bu}})]@Au$ were examined (Figure 3 insert). Retention of SMM behavior on immobilization of this SMM on the Au NPs is confirmed by the observation of non-zero and frequency-dependent out-of-phase component (χ_g'') below 4 K. The maxima of χ_g'' are below the temperature limit of the magnetometer which precluded determination of the barrier height associated with the process and comparison to that for free $[\text{Cu}_3\text{Tb}(\text{L}^{\text{Bu}})]$ ($U_{\text{eff}} = 19.5$ K; no dc field). Similar to the free $[\text{Cu}_3\text{Tb}(\text{L}^{\text{Bu}})]$, the application of a weak dc field during these ac measurements made virtually no difference to the relaxation data. The relaxation in $[\text{Cu}_3\text{Tb}(\text{L}^{\text{Bu}})]@Au$ is somewhat faster than in the pristine $[\text{Cu}_3\text{Tb}(\text{L}^{\text{Bu}})]$, in which the out-of-phase component becomes non-zero above 6 K and the maxima of the peaks are within the window of the measurement. This is probably due to slight modification of the environment of the Tb^{III} ions resulting from grafting to ALA@Au. It should be noted that ALA@Au shows a complete absence of an out-of-phase component down to 1.8 K (Figure S10, SI).

In conclusion, we have generated 3.6 ± 0.7 nm diameter Au NPs pre-functionalized with appropriate linkers, ALA@Au, then covalently grafted the robust macrocyclic SMM $[\text{Cu}_3\text{Tb}(\text{L}^{\text{Bu}})]$ onto them, creating the hybrid material $[\text{Cu}_3\text{Tb}(\text{L}^{\text{Bu}})]@Au$. The $[\text{Cu}_3\text{Tb}(\text{L}^{\text{Bu}})]$ is shown to be intact on the NP surface (XPS, XAS and XMCD) and standard SQUID measurements reveal that the slow relaxation of magnetism of pure $[\text{Cu}_3\text{Tb}(\text{L}^{\text{Bu}})]$ is preserved after immobilization on the NPs. This proof of principle study also demonstrates an important extension of the microemulsion method to the formation of small monodisperse NPs coated with functionalized linkers (rather than the aliphatic coatings used previously), which in turn opens up access to a far wider range of hybrid materials and associated applications than could hitherto have been imagined.

This proof of principle study provides a far more versatile strategy to such hybrids than those previously reported, as it is not necessary to synthetically modify each complex prior to immobilization, and the samples can be studied by standard techniques.

This opens the way to systematic studies of a range of Au NP-immobilized complexes.

ASSOCIATED CONTENT

Supporting Information

Experimental details, details of calculations and supplementary magnetism data. This material is available free of charge via the Internet at <http://pubs.acs.org>.

AUTHOR INFORMATION

Corresponding Author

*sbrooker@chemistry.otago.ac.nz

Author Contributions

All authors have given approval to the final version of the manuscript.

Notes

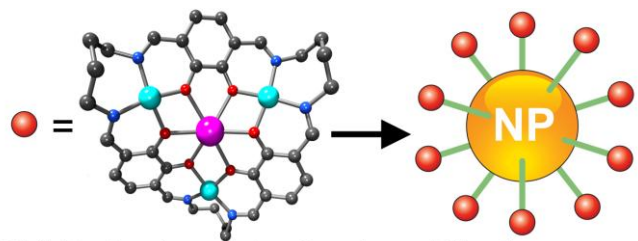
The authors declare no competing financial interests.

ACKNOWLEDGMENT

This work was supported by the University of Otago, the MacDiarmid Institute for Advanced Materials and Nanotechnology and the Marsden Fund (RSNZ). Ente Cassa di Risparmio di Firenze is acknowledged for funding CeTeCS activities.

REFERENCES

- (1) Gatteschi, D.; Sessoli, R.; Villain, F. *Molecular Nanomagnets*; Oxford University Press: Oxford, 2006.
- (2) Aromí, G.; Brechin, E. K. *Struct. Bond.* **2006**, *122*, 1-67; Sessoli, R.; Powell, A. K. *Coord. Chem. Rev.* **2009**, *253*, 2328-2341; Andruh, M.; Costes, J.-P.; Diaz, C.; Gao, S. *Inorg. Chem.* **2009**, *48*, 3342-3359; Murrie, M. *Chem. Soc. Rev.* **2010**, *39*, 1986-1995; Glaser, T. *Chem. Commun.* **2011**, *47*, 116-130; Rinehart, J. D.; Long, J. R. *Chem. Sci.* **2011**, *2*, 2078-2085; Luzona, J.; Sessoli, R. *Dalton Trans.* **2012**, *41*, 13556-13567; Woodruff, D. N.; Winpenny, R. E. P.; Layfield, R. A. *Chem. Rev.* **2013**, *113*, 5110-5148; Layfield, R. A. *Organometallics* **2014**, *33*, 1084-1099; Feltham, H. L. C.; Brooker, S. *Coord. Chem. Rev.* **2014**, *276*, 1-33; Liu, K.; Shi, W.; Cheng, P. *Coord. Chem. Rev.* **2014**, *289-290*, 74-122; Pedersen, K. S.; Bendix, J.; Clérac, R. *Chem. Commun.* **2014**, *50*, 4396-4415; Glaser, T.; Hoeke, V.; Gieb, K.; Schnack, J.; Schröder, C.; Müller, P. *Coord. Chem. Rev.* **2015**; Happ, P.; Plenck, C.; Rentschler, E. *Coord. Chem. Rev.* **2015**, *289*, 238-260; Zhang, P.; Zhang, L.; Tang, J. *Dalton Trans.* **2015**, *44*, 3923-3929; Meihaus, K. R.; Long, J. R. *Dalton Trans.* **2015**, *44*, 2517-2528; Dhers, S.; Feltham, H. L. C.; Brooker, S. *Coord. Chem. Rev.* **2015**, *296*, 24-44.
- (3) Gatteschi, D.; Cornia, A.; Mannini, M.; Sessoli, R. *Inorg. Chem.* **2009**, *48*, 3408-3419; Holmberg, R.; Murugesu, M. *J. Mat. Chem. C* **2015**, *3*, 11986-11998.
- (4) Wang, H.; Wang, B.-W.; Bian, Y.; Gao, S.; Jiang, J. *Coord. Chem. Rev.* **2016**, *306*, Part 1, 195-216; Bertani, F.; Cristiani, N.; Mannini, M.; Pinalli, R.; Sessoli, R.; Dalcanale, E. *Eur. J. Org. Chem.* **2015**, *2015*, 7036-7042; Mannini, M.; Bertani, F.; Tudisco, C.; Malavolti, L.; Poggini, L.; Misztal, K.; Menozzi, D.; Motta, A.; Otero, E.; Ohresser, P.; Sainctavit, P.; Condorelli, G. G.; Dalcanale, E.; Sessoli, R. *Nature Commun.* **2014**, *5*, 4582.
- (5) Condorelli, G. G.; Motta, A.; Pellegrino, G.; Cornia, A.; Gorini, L.; Fragalà, I. L.; Sangregorio, C.; Sorace, L. *Chem. Mater.* **2008**, *20*, 2405-2411; Mannini, M.; Pineider, F.; Sainctavit, P.; Danieli, C.; Otero, E.; Sciancalepore, C.; Talarico, A. M.; Arrio, M.-A.; Cornia, A.; Gatteschi, D.; Sessoli, R. *Nature Materials* **2009**, *8*, 194 - 197; Malavolti, L.; Lanzilotto, V.; Ninova, S.; Poggini, L.; Cimatti, I.; Cortigiani, B.; Margheriti, L.; Chiappe, D.; Otero, E.; Sainctavit, P.; Totti, F.; Cornia, A.; Mannini, M.; Sessoli, R. *Nano Letters* **2015**, *15*, 535-541; Totaro, P.; Poggini, L.; Favre, A.; Mannini, M.; Sainctavit, P.; Cornia, A.; Magnani, A.; Sessoli, R. *Langmuir* **2014**, *30*, 8645-8649; Mannini, M.; Tancini, E.; Sorace, L.; Sainctavit, P.; Arrio, M. A.; Qian, Y.; Otero, E.; Chiappe, D.; Margheriti, L.; Cezar, J. C.; Sessoli, R.; Cornia, A. *Inorg. Chem.* **2011**, *50*, 2911-2917
- (6) Mannini, M.; Pineider, F.; Danieli, C.; Totti, F.; Sorace, L.; Sainctavit, P.; Arrio, M.-A.; Otero, E.; Joly, L.; Cezar, J. C.; Cornia, A.; Sessoli, R. *Nature* **2010**, *468*, 417-422.
- (7) Perfetti, M.; Pineider, F.; Poggini, L.; Otero, E.; Mannini, M.; Sorace, L.; Sangregorio, C.; Cornia, A.; Sessoli, R. *Small* **2014**, *10*, 323-329.
- (8) Cornia, A.; Mannini, M.; Sainctavit, P.; Sessoli, R. *Chem. Soc. Rev.* **2011**, *40*, 3076-3091.
- (9) Cornia, A.; Mannini, M. *Struct. Bond.* **2015**, *164*, 293-330.
- (10) Holmberg, R. J.; Hutchings, A.-J.; Habib, F.; Korobkov, I.; Scaiano, J. C.; Murugesu, M. *Inorg. Chem.* **2013**, *52*, 14411-14418.
- (11) Feltham, H. L. C.; Lan, Y.; Klöwer, F.; Ungur, L.; Chibotaru, L. F.; Powell, A. K.; Brooker, S. *Chemistry - A European Journal* **2011**, *17*, 4362-4365 and cover feature; Feltham, H. L. C.; Clérac, R.; Powell, A. K.; Brooker, S. *Inorg. Chem.* **2011**, *50*, 4232-4234; Feltham, H. L. C.; Klöwer, F.; Cameron, S. A.; Larsen, D. S.; Lan, Y.; Tropiano, M.; Faulkner, S.; Powell, A. K.; Brooker, S. *Dalton Trans.* **2011**, *40*, 11425-11432; Feltham, H. L. C.; Clérac, R.; Ungur, L.; Vieru, V.; Chibotaru, L. F.; Powell, A. K.; Brooker, S. *Inorg. Chem.* **2012**, *51*, 10603-10612; Feltham, H. L. C.; Dhers, S.; Rouzières, M.; Clérac, R.; Powell, A. K.; Brooker, S. *Inorganic Chemistry Frontiers* **2015**, *2*, 982-990 and front cover feature.
- (12) Feltham, H. L. C.; Clérac, R.; Ungur, L.; Chibotaru, L. F.; Powell, A. K.; Brooker, S. *Inorg. Chem.* **2013**, *52*, 3236-3240.
- (13) Fleury, B.; Catala, L.; Huc, V.; David, C.; Zhao Zhong, W.; Jegou, P.; Baraton, L.; Palacin, S.; Albouy, P.-A.; Mallah, T. *Chem. Commun.* **2005**, 2020-2022.
- (14) Coronado, E.; Forment-Aliaga, A.; Romero, F. M.; Corradini, V.; Biagi, R.; De Renzi, V.; Gambardella, A.; del Pennino, U. *Inorg. Chem.* **2005**, *44*, 7693-7695.
- (15) Schulman, J. H.; Stoeckenius, W.; Prince, L. M. *J. Phys. Chem.* **1959**, *63*, 1677-1680.
- (16) Garden, A. L.; van der Salm, L.; Schwass, D. R.; Meledandri, C. J. *RSC Adv.* **2013**, *3*, 2192-2196.
- (17) Ghosh, S. K.; Pal, T. *Chem. Rev.* **2007**, *107*, 4797-4862.



SMM behavior retained on immobilization
